Thermo-optical effects in high-power Ytterbium-doped fiber amplifiers

Hansen, Kristian Rymann; Alkeskjold, Thomas Tanggaard; Broeng, Jes; Lægsgaard, Jesper

Published in:
Optics Express

Link to article, DOI:
10.1364/OE.19.023965

Publication date:
2011

Document Version
Publisher's PDF, also known as Version of record

Thermo-optical effects in high-power Ytterbium-doped fiber amplifiers

Kristian Rymann Hansen,[1,*] **Thomas Tanggaard Alkeskjold,**[2] **Jes Broeng,**[2] **and Jesper Lægsgaard**[1]

[1]*Department of Photonics Engineering, Technical University of Denmark Bldg. 345v, DK-2800 Kgs. Lyngby, Denmark*

[2]*NKT Photonics A/S, Blokken 84, DK-3460 Birkerød, Denmark*

[*]*kryh@fotonik.dtu.dk*

Abstract: We investigate the effect of temperature gradients in high-power Yb-doped fiber amplifiers by a numerical beam propagation model, which takes thermal effects into account in a self-consistent way. The thermally induced change in the refractive index of the fiber leads to a thermal lensing effect, which decreases the effective mode area. Furthermore, it is demonstrated that the thermal lensing effect may lead to effective multi-mode behavior, even in single-mode designs, which could possibly lead to degradation of the output beam quality.

OCIS codes: (060.2320) Fiber optics amplifiers and oscillators; (060.4370) Nonlinear optics, fibers; (350.6830) Thermal lensing.

References and links

1. Y. Jeong, J. K. Sahu, D. N. Payne, and J. Nilsson, "Ytterbium-doped large-core fiber laser with 1.36 kW continuous-wave output power," Opt. Express **12**, 6088–6092 (2004).
2. D. Gapontsev, "6 kW CW single mode Ytterbium fiber laser in all-fiber format," in *Proc. Solid State and Diode Laser Technology Review* (2008).
3. J. Li, K. Duan, Y. Wang, X. Cao, W. Zhao, Y. Guo, and X. Lin, "Theoretical analysis of the heat dissipation mechanism in Yb^{3+}-doped double-clad fiber lasers," J. Mod. Opt. **55**, 459–471 (2008).
4. J. Limpert, T. Schreiber, A. Liem, S. Nolte, H. Zellmer, T. Perschel, V. Guyenot, and A. Tünnermann, "Thermo-optical properties of air-clad photonic crystal fiber lasers in high power operation," Opt. Express **11**, 2982–2990 (2003).
5. S. Hädrich, T. Schreiber, T. Pertsch, J. Limpert, T. Peschel, R. Eberhardt, and A. Tünnermann, "Thermo-optical behavior of rare-earth-doped low-NA fibers in high power operation," Opt. Express **14**, 6091–6097 (2006).
6. J. Limpert, F. Röser, D. N. Schimpf, E. Seise, T. Eidam, S. Hädrich, J. Rothhardt, C. J. Misas, and A. Tünnermann, "High Repetition Rate Gigawatt Peak Power Fiber Laser Systems: Challenges, Design, and Experiment," IEEE J. Sel. Topics Quantum Electron. **15**, 159–169 (2009).
7. T. Eidam, S. Hanf, E. Seise, T. V. Andersen, T. Gabler, C. Wirth, T. Schreiber, J. Limpert, and A. Tünnermann, "Femtosecond fiber CPA system emitting 830 W average output power," Opt. Lett. **35**, 94–96 (2010).
8. F. Stutzki, F. Jansen, T. Eidam, A. Steinmetz, C. Jauregui, J. Limpert, and A. Tünnermann, "High average power large-pitch fiber amplifier with robust single-mode operation," Opt. Lett. **36**, 689–691 (2011).
9. T. Eidam, C. Wirth, C. Jauregui, F. Stutzki, F. Jansen, H. Otto, O. Schmidt, T. Schreiber, J. Limpert, and A. Tünnermann, "Experimental observations of the threshold-like onset of mode instabilities in high power fiber amplifiers," Opt. Express **19**, 13218–13224 (2011).
10. C. Jauregui, T. Eidam, J. Limpert, and A. Tünnermann, "The impact of modal interference on the beam quality of high-power fiber amplifiers," Opt. Express **19**, 3258–3271 (2011).
11. A. V. Smith, and J. J. Smith, "Mode instability in high power fiber amplifiers," Opt. Express **19**, 10180–10192 (2011).
12. M. Koshiba, and K. Saitoh, "Applicability of classical optical fiber theories to holey fibers," Opt. Lett. **29**, 1739–1741 (2004).
13. R. W. Boyd, *Nonlinear Optics*, 3rd. ed. (Elsevier 2008).

#152482 - $15.00 USD Received 5 Aug 2011; revised 19 Sep 2011; accepted 13 Oct 2011; published 10 Nov 2011

14. P. W. Milonni, and J. H. Eberly, *Lasers* (John Wiley & Sons 1988).
15. D. E. McCumber, "Einstein Relations Connecting Broadband Emission and Absorption Spectra," Phys. Rev. **136**, A954–A957 (1964).
16. G. R. Hadley, "Transparent boundary condition for beam propagation," Opt. Lett. **16**, 624–626 (1991).
17. W. H. Press, B. P. Flannery, S. A. Teukolsky, and W. T. Vetterling, *Numerical Recipes in Pascal* (Cambridge University Press 1989).
18. S. Wielandy, "Implications of higher-order mode content in large mode area fibers with good beam quality," Opt. Express **15**, 15402–15409 (2007).

1. Introduction

Recent development in high-power Yb-doped fiber amplifiers have lead to significant increases in operating power, and CW output power of a few kW have been demonstrated [1, 2]. Although Yb-doped fiber amplifiers have excellent heat dissipation properties owing to the large surface-to-volume ratio of the fiber, significant heating of the core occurs during high average power operation due to the quantum defect associated with the gain medium. Previous work has investigated the heat dissipation mechanism [3] and the effect of a specified thermal load on the transverse mode properties of fiber lasers and amplifiers [4, 5], and recent publications have discussed limiting factors for the power-scalability of fiber amplifiers, such as self-phase-modulation (SPM) in high peak power pulsed systems [6] and mode instability issues at high average power [7–9]. Numerical studies have attributed the latter effect to thermal and population inversion induced coupling between the fundamental and a higher order mode of a multi-mode fiber [10, 11].

In this paper we present a numerical model, based on a beam propagation code, that includes the non-linear interaction between the temperature distribution generated by the signal gain and the transverse field profile, which is influenced by the temperature induced change in refractive index. We have used this model to study the thermo-optical effects in large mode area (LMA) step-index fiber (SIF) amplifiers under high-power operation. In particular, we focus on two effects related to the above mentioned scalability limitations: The thermal lensing effect, which leads to beam self-focusing and hence to increased SPM, and an effective multi-mode behavior which can occur at high power even in fibers which are single-mode by design. We believe the latter effect lies at the core of the beam instability issues reported in [7, 8]. Contrary to the investigations of Jauregui *et al.* [10] and Smith *et al.* [11], we focus on single-mode fibers and show that the thermal effect in itself is sufficient to induce a multi-moded behavior.

Many state-of-the-art rare-earth doped fiber amplifiers are based on photonic crystal fibers (PCF), the simulation of which require computationally demanding full 3D beam propagation models. In order to make the calculations less demanding, we have chosen to model SIFs, but since simple index-guiding PCFs are well approximated by an effective SIF [12], we expect our results to be applicable to such fibers as well.

Our paper is arranged as follows: In section 2 we describe the details of our numerical model, and discuss advantages and limitations. In section 3 we present the results of our numerical investigation of the thermo-optical effect for various fiber design parameters, and discuss the implications for the design of high-power fiber amplifiers.

2. Numerical method

Our beam propagation algorithm simulates double-clad Yb-doped SIF amplifiers. Since we will deal mainly with single-mode fibers in this paper, we can assume that the electromagnetic field of the signal is cylindrically symmetric. This drastically reduces the numerical complexity of the problem and leads to a very efficient numerical solution. This is particularly important for modeling backward pumped amplifiers, since the required initial condition for the pump power is not known a priori in this case, and thus requires the beam propagation code to be run

#152482 - $15.00 USD Received 5 Aug 2011; revised 19 Sep 2011; accepted 13 Oct 2011; published 10 Nov 2011

iteratively to obtain the desired input pump power. This assumption, however, also imposes the limitation that we cannot consider an input beam profile which is shifted or tilted relative to the symmetry axis of the fiber. Our method can be extended to handle non-symmetric cases by expanding the azimuthal dependence of the field in a Fourier series, which will be the subject of a later publication.

The electric field of the signal can be written

$$\mathbf{E}_s(\mathbf{r},t) = \mathbf{u}_s E_s(r,z) e^{i(\beta z - \omega_s t)}, \tag{1}$$

where $\mathbf{u}_s$ is the polarization unit vector, E_s is the slowly varying envelope of the signal field, β is an estimate of the propagation constant of the fundamental mode and ω_s is the carrier angular frequency of the signal. In the scalar approximation, the field envelope E_s obeys the paraxial wave equation

$$\frac{\partial E_s}{\partial z} = \frac{i}{2\beta}\left[\frac{\partial^2 E_s}{\partial r^2} + \frac{1}{r}\frac{\partial E_s}{\partial r} + \left(k_0^2\left[\varepsilon(r) + \Delta\varepsilon(r,z)\right] - \beta^2\right)E_s + \mu_0\omega_s^2 p(r,z)\right]. \tag{2}$$

The first terms on the right hand side of Eq. (2) describe the propagation of the signal field, with vacuum wavenumber k_0, in a fiber with a relative permittivity distribution given by ε. The perturbation of this permittivity distribution due to heating of the core is given by $\Delta\varepsilon$. The last term describes the effect of the Ytterbium doping, which gives rise to an induced polarization $\mathbf{P}_{Yb}$ given by a slowly varying envelope p as

$$\mathbf{P}_{Yb}(\mathbf{r},t) = \mathbf{u}_s p(r,z) e^{i(\beta z - \omega_s t)}. \tag{3}$$

In this paper we assume that the fiber is cladding pumped at a wavelength of 975 nm and that the signal wavelength is close to 1030 nm. In this case the Yb^{3+} ions can be modeled as the quasi-three-level system shown in Fig. 1.

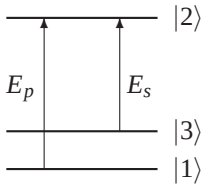

Fig. 1. Simplified energy level diagram for Yb^{3+}.

The equations of motion for the slowly varying density matrix elements $\sigma_{\mu\nu}$ are [13]:

$$\dot{\sigma}_{11} = \frac{i}{\hbar}\left(\mu_{12}E_p^*\sigma_{21} - \text{c.c.}\right) + \gamma_{21}\sigma_{22} + \overline{\gamma}_{31}\sigma_{33} - \overline{\gamma}_{13}\sigma_{11} \tag{4a}$$

$$\dot{\sigma}_{22} = -\frac{i}{\hbar}\left(\mu_{12}E_p^*\sigma_{21} + \mu_{32}E_s^*\sigma_{23} - \text{c.c.}\right) - \left(\gamma_{23} + \gamma_{21}\right)\sigma_{22} \tag{4b}$$

$$\dot{\sigma}_{33} = \frac{i}{\hbar}\left(\mu_{32}E_s^*\sigma_{23} - \text{c.c.}\right) + \gamma_{23}\sigma_{22} - \overline{\gamma}_{31}\sigma_{33} + \overline{\gamma}_{13}\sigma_{11} \tag{4c}$$

$$\dot{\sigma}_{21} = \frac{i}{\hbar}\left(\mu_{12}^*E_p\left(\sigma_{11} - \sigma_{22}\right) + \mu_{32}^*E_s\sigma_{31}\right) - \tilde{\Gamma}_{21}\sigma_{21} \tag{4d}$$

$$\dot{\sigma}_{23} = \frac{i}{\hbar}\left(\mu_{32}^*E_s\left(\sigma_{33} - \sigma_{22}\right) + \mu_{12}^*E_p\sigma_{31}^*\right) - \tilde{\Gamma}_{23}\sigma_{23} \tag{4e}$$

$$\dot{\sigma}_{31} = \frac{i}{\hbar}\left(\mu_{32}E_s^*\sigma_{21} - \mu_{12}^*E_p\sigma_{23}^*\right) - \tilde{\Gamma}_{31}\sigma_{31}, \tag{4f}$$

#152482 - $15.00 USD Received 5 Aug 2011; revised 19 Sep 2011; accepted 13 Oct 2011; published 10 Nov 2011

where $\mu_{\mu\nu}$ are the matrix elements of the dipole moment operator, E_p is the pump field envelope, $\gamma_{\mu\nu}$ are spontaneous emission rates from state μ into state ν and the non-radiative transition rates are denoted $\bar{\gamma}_{\mu\nu}$. The complex dephasing rates $\tilde{\Gamma}_{\mu\nu}$ of the coherences are given by

$$\tilde{\Gamma}_{21} = \tilde{\gamma}_{21} - i\Delta_p \tag{5a}$$

$$\tilde{\Gamma}_{23} = \tilde{\gamma}_{23} - i\Delta_s \tag{5b}$$

$$\tilde{\Gamma}_{31} = \tilde{\gamma}_{31} - i\Delta_2, \tag{5c}$$

where $\tilde{\gamma}_{\mu\nu}$ are the real dephasing rates of the coherences $\sigma_{\mu\nu}$, $\Delta_p = \omega_p - \omega_{21}$ is the pump detuning, $\Delta_s = \omega_s - \omega_{23}$ is the signal detuning and $\Delta_2 = \Delta_p - \Delta_s$ is the two-photon detuning of the pump and signal. Since the dephasing rates $\tilde{\gamma}_{\mu\nu}$ in Eq. (4) are large, we can adiabatically eliminate the coherences [14], which leads to a rate equation for the excited state population

$$\dot{\sigma}_{22} = B_p(\Delta_p)|E_p|^2(\sigma_{11} - \sigma_{22}) + B_s(\Delta_s)|E_s|^2(\sigma_{33} - \sigma_{22}) - (\gamma_{23} + \gamma_{21})\sigma_{22}, \tag{6}$$

where

$$B_p = \frac{2\tilde{\gamma}_{21}|\mu_{12}|^2}{\hbar^2\left(\tilde{\gamma}_{21}^2 + \Delta_p^2\right)} \quad \text{and} \quad B_s = \frac{2\tilde{\gamma}_{23}|\mu_{32}|^2}{\hbar^2\left(\tilde{\gamma}_{23}^2 + \Delta_s^2\right)}. \tag{7}$$

Analogous to the McCumber theory [15], we assume that the two lower states remain in thermal equilibrium. Denoting the total population of the two lower states as $\rho_1 = \sigma_{11} + \sigma_{33}$ and the excited state population as $\rho_2 = \sigma_{22}$, we arrive at a rate equation for the excited state population. In the steady-state, this equation becomes

$$\rho_2(r,z) = \frac{\sigma_{ap}\Phi_p(z) + \sigma_{as}\Phi_s(r,z)}{(\sigma_{ap} + \sigma_{ep})\Phi_p(z) + (\sigma_{as} + \sigma_{es})\Phi_s(r,z) + \gamma}, \tag{8}$$

where Φ_p and Φ_s denote the pump and signal photon flux density, respectively, and $\gamma = \gamma_{21} + \gamma_{23}$ is the total spontaneous emission rate of the excited state. In our simplified 3-level model, the absorption and emission cross sections at the signal wavelength, σ_{as} and σ_{es}, are given by

$$\sigma_{as}(\omega_s) = \frac{e^{-\Delta E/k_B T}}{1 + e^{-\Delta E/k_B T}} \frac{\hbar\omega_s B_s}{2\varepsilon_0 c n_c} \quad \text{and} \quad \sigma_{es}(\omega_s) = \frac{\hbar\omega_s B_s}{2\varepsilon_0 c n_c}, \tag{9}$$

while at the pump wavelength, the absorption and emission cross sections are

$$\sigma_{ap}(\omega_p) = \frac{1}{1 + e^{-\Delta E/k_B T}} \frac{\hbar\omega_p B_p}{2\varepsilon_0 c n_c} \quad \text{and} \quad \sigma_{ep}(\omega_p) = \frac{\hbar\omega_p B_p}{2\varepsilon_0 c n_c}. \tag{10}$$

Here ΔE is the energy difference between states 1 and 3.

The induced polarization at the signal wavelength is determined by the coherence σ_{23} and is given in terms of the signal field and population inversion as

$$p(r,z) = \frac{\varepsilon_0 n_c \rho_{Yb}(r)}{k_0}\left(i + \frac{\Delta_s}{\tilde{\gamma}_{23}}\right)\left[\sigma_{as}(\omega_s) - \left[\sigma_{as}(\omega_s) + \sigma_{es}(\omega_s)\right]\rho_2(r,z)\right]E_s(r,z), \tag{11}$$

where n_c is the core refractive index and ρ_{Yb} is the density of Ytterbium ions. As discussed in [10], this induced polarization can lead to a change in the refractive index which depends on the population inversion. In our simplified model this happens when the signal is detuned from resonance ($\Delta_s \neq 0$), and an estimate of the magnitude of this effect when $\Delta_s = \tilde{\gamma}_{23}/2$ and $\rho_2 = 0.5$ yields $\Delta\varepsilon \approx 10^{-6}$, which is quite small compared to the thermally induced changes in the refractive index. We therefore ignore this effect in our calculations.

#152482 - $15.00 USD Received 5 Aug 2011; revised 19 Sep 2011; accepted 13 Oct 2011; published 10 Nov 2011

Inserting Eq. (11) into Eq. (2) and assuming $|\Delta_s| \ll \tilde{\gamma}_{23}$ yields a beam propagation equation which includes the signal gain due to the Ytterbium doping

$$\frac{\partial E_s}{\partial z} = \frac{i}{2\beta}\left(\frac{\partial^2 E_s}{\partial r^2} + \frac{1}{r}\frac{\partial E_s}{\partial r} + \left(k_0^2(\varepsilon+\Delta\varepsilon) - \beta^2\right)E_s\right) + \frac{\sqrt{\varepsilon}k_0\rho_{Yb}}{2\beta}\left(\sigma_{es}\rho_2 - (1-\rho_2)\sigma_{as}\right)E_s. \tag{12}$$

The radial coordinate is discretized using a second order finite-difference scheme, and a transparent boundary condition [16] is applied at the surface. The signal field can then be propagated forward in z from an initial beam profile $E_s(0,r)$ using a split-operator approach

$$E_s(z+\Delta z, r) \approx \exp\left(\frac{\Delta z}{2}\hat{R}\right)\exp\left(\Delta z\hat{N}\right)\exp\left(\frac{\Delta z}{2}\hat{R}\right)E_s(z,r), \tag{13}$$

where the operators $\hat{R}$ and $\hat{N}$ are given by

$$\hat{R}E_s = \frac{i}{2\beta}\left(\frac{\partial^2 E_s}{\partial r^2} + \frac{1}{r}\frac{\partial E_s}{\partial r}\right), \tag{14}$$

$$\hat{N}E_s = \left[-\frac{\rho_{Yb}}{2}\sqrt{\frac{\varepsilon}{\varepsilon_{eff}}}\left(\sigma_{as} - (\sigma_{as}+\sigma_{es})\rho_2\right) + \frac{ik_0^2}{2\beta}\left(\varepsilon+\Delta\varepsilon-\varepsilon_{eff}\right)\right]E_s, \tag{15}$$

and $\varepsilon_{eff} = \beta^2/k_0^2$. The input signal beam profile is taken to be the Gaussian

$$E_s(0,r) = \frac{P_s(0)}{\pi\varepsilon_0 c n_c w^2}e^{-r^2/w^2}, \tag{16}$$

where w is the characteristic radius of the input beam, which is chosen to be equal to the core radius, and $P_s(0)$ is the input signal power.

To calculate the relative permittivity perturbation $\Delta\varepsilon$ due to heating of the fiber under high-power operation, we solve the steady-state heat equation under the assumption that the longitudinal temperature gradient is much smaller than the radial temperature gradient

$$\frac{\partial^2\Delta T}{\partial r^2} + \frac{1}{r}\frac{\partial\Delta T}{\partial r} = -\frac{Q}{\kappa}. \tag{17}$$

Here ΔT is the temperature increase relative to the temperature of the coolant, κ is the thermal conductivity of the fiber and the thermal load Q is given by

$$Q = \rho_{Yb}\hbar(\omega_p - \omega_s)\left(\Phi_s\left(\sigma_{es}\rho_2 - \sigma_{as}\rho_1\right) + \gamma_{23}\rho_2\right), \tag{18}$$

where ω_p is the pump angular frequency. The first term in this expression represents heat generated by non-radiative relaxation following stimulated emission of signal photons and is the dominant heat source, whereas the last, much smaller, term is due to non-radiative relaxation following spontaneous emission at the signal wavelength. We assume uniform efficient water cooling of the fiber and thus apply a simple Dirichlet boundary condition $\Delta T = 0$ at the outer boundary when solving the heat equation. The temperature induced change of the refractive index of the fiber is given by the simple linear relationship $\Delta\varepsilon = \eta\Delta T$, where the thermal sensitivity $\eta = 3.5\times10^{-5}$ K^{-1}.

Since we are modeling cladding pumped fiber amplifiers, we assume that the pump intensity is constant over the core. We can thus model the propagation of the pump by the simple ordinary differential equation

$$\frac{\mathrm{d}P_p}{\mathrm{d}z} = \pm\frac{2\pi}{A_{cl}}P_p(z)\int_0^{R_c}\rho_{Yb}(r)\left[\sigma_{ap} - (\sigma_{ap}+\sigma_{ep})\rho_2(r,z)\right]r\mathrm{d}r, \tag{19}$$

#152482 - $15.00 USD Received 5 Aug 2011; revised 19 Sep 2011; accepted 13 Oct 2011; published 10 Nov 2011

where P_p is the pump power, A_{cl} is the area of the inner cladding and R_c is the radius of the doped core. The positive sign applies to forward pumping whereas the negative sign applies to backward pumping. The pump power can thus be propagated in the z direction from its initial value $P_p(0)$ by the equation

$$P_p(z+\Delta z) \approx P_p(z) \pm \frac{2\pi}{A_{cl}} P_p(z) \Delta z \int_0^{R_c} \rho_{Yb}(r) \left[\sigma_{ap} - (\sigma_{ap} + \sigma_{ep}) \rho_2(r,z)\right] r \mathrm{d}r. \tag{20}$$

The beam propagation algorithm can be summarized by the following steps:

1. Compute the excited state population ρ_2 from Eq. (8).
2. Compute ΔT by solving Eq. (17) and calculate $\Delta\varepsilon$.
3. Propagate the signal field one step in z by applying Eq. (13).
4. Propagate the pump field one step in z by applying Eq. (20).

These steps are carried out until the signal has been propagated the desired distance. In the case of backward pumping an initial guess for the initial condition of the pump power $P_p(0)$ must be provided, and the entire beam propagation algorithm is run iteratively until the desired input pump power $P_p(L)$ is obtained. After each run the pump initial condition $P_p(0)$ is adjusted according to a simple secant method [17]. With a tolerance of 1% of the desired input pump power and a reasonable estimate of the pump initial condition, only a few iterations of the beam propagation algorithm are required.

3. Numerical results

We have used our numerical model to investigate two important effects of the radial thermal gradient produced in the fiber under high-power operation. The first effect is thermal lensing, which leads to focusing of the signal beam, and the second is the thermally induced multi-mode behavior of the amplifier. Although we are considering double-clad fibers, we have chosen to model the fibers as SIFs without the large index contrast associated with the pump cladding, and simply assume that the pump light is confined to a given inner cladding diameter. This is done in order to allow any signal radiation modes to escape the computational domain via the transparent boundary condition and thereby obtain an ideal picture of the guided signal field. In actual double-clad fibers, these radiation modes would predominantly be cladding modes which can interfere with the guided signal, but since such cladding modes are only weakly amplified due to their small overlap with the Yb-doped core, their influence on the guided signal is small. In double-clad PCF amplifiers, the pump light is confined by large air holes. While it is not clear that such a structure can be adequately approximated by a step-index model, we believe that its influence on the guided signal is negligible, provided that the pump cladding diameter is sufficiently large to prevent a significant overlap between the guided signal and the air holes.

3.1. Thermal lensing

One of the main advantages of LMA fiber amplifiers is the lower intensity of the guided mode, which allows for a higher signal power before detrimental non-linear effects such as SPM becomes a limiting factor. These effects are most important in pulsed operation where the peak power is high. Although our model assumes CW operation, we can use the model to estimate the thermal lensing effect induced during pulsed operation at high repetition rates. We quantify the thermal lensing effect by calculating the so-called B-integral as it has been demonstrated to

#152482 - $15.00 USD Received 5 Aug 2011; revised 19 Sep 2011; accepted 13 Oct 2011; published 10 Nov 2011

give a useful estimate of the severity of non-linear effects such as SPM [6]. It is given by

$$B = \frac{2\pi n_2}{\lambda_s} \int_0^L \frac{P_s(z)}{A_{eff}(z)} \mathrm{d}z, \tag{21}$$

where n_2 is the non-linear refractive index of Silica, P_s is the average signal power and A_{eff} is the effective area of the signal beam

$$A_{eff}(z) = 2\pi \frac{\left(\int_0^\infty |E(z,r)|^2 r \mathrm{d}r\right)^2}{\int_0^\infty |E(z,r)|^4 r \mathrm{d}r}. \tag{22}$$

We have simulated a 1 m long double-clad fiber amplifier, in the following referred to as Fiber A, with a core diameter of 40 μm, an inner cladding diameter of 200 μm and an outer diameter of 400 μm. The core-cladding index step is 10^{-4}, which gives $V \approx 2.08$ at the signal wavelength of 1030 nm, and the Yb doping in the core is 10^8 $\mu\mathrm{m}^{-3}$. The fiber is cladding pumped at 975 nm, and we have varied the input pump power between approximately 50 W - 5 kW. The signal input power was kept fixed at 1 W, and both forward and backward pumping was simulated. Figure 2 shows the pump and signal power as a function of distance along the fiber for forward and backward pumping with 1 kW input pump power and 1 W input signal power. The pump is efficiently depleted due to the high Yb doping which results in a high

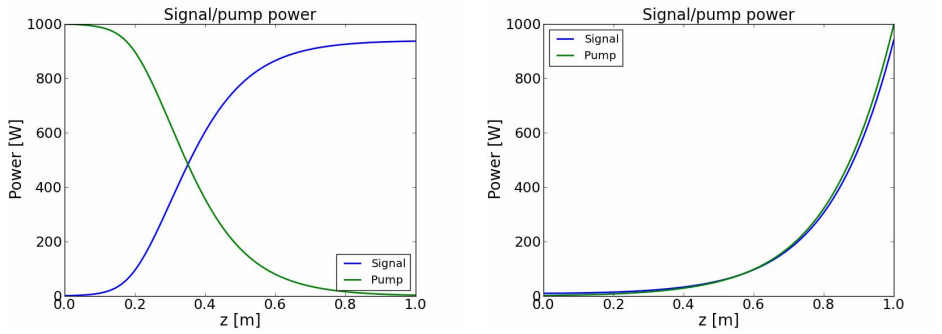

(a) Forward pumping (b) Backward pumping

Fig. 2. Signal and pump power as a function of z for (a) forward pumping and (b) backward pumping of Fiber A.

efficiency close to the quantum limit.

Figure 3 shows the excited state population ρ_2 of Yb as a function of longitudinal and radial distance for Fiber A at 1 kW pump power. The effect of transverse hole burning is clearly seen, especially in the backward pumped case.

The heating of the fiber occurs where the stimulated emission is largest. This is clearly evident from Fig. 4, which shows the temperature increase as a function of z and r for Fiber A at 1 kW pump power. The heating of the core creates a large radial thermal gradient in the fiber, which leads to a thermal lensing effect that causes the beam area to decrease, as shown in Fig. 5. It is also clear from Fig. 4 that the temperature increase is much larger in the backward pumped case due to the large gain near the output end of the fiber.

As is clear from Eq. (21), the self-focusing of the beam results in a higher value of the B-integral. In Fig. 6 we show the B-integral as a function of input pump power for both forward and backward pumped configurations. The dashed lines show the result when the thermal sensitivity η is set to zero. For comparison, we have also simulated a fiber (Fiber B), identical to

#152482 - $15.00 USD Received 5 Aug 2011; revised 19 Sep 2011; accepted 13 Oct 2011; published 10 Nov 2011

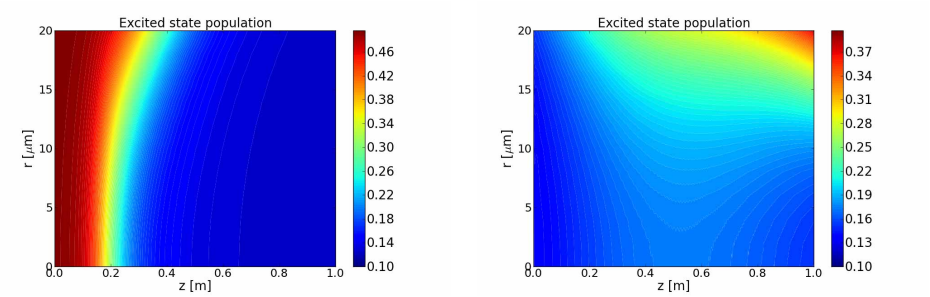

(a) Forward pumping (b) Backward pumping

Fig. 3. Excited state population as a function of z and r for (a) forward pumping and (b) backward pumping of Fiber A at 1 kW pump power and 1 W input signal power.

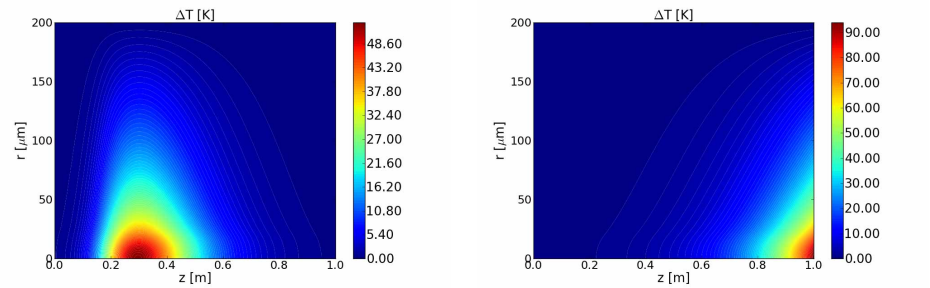

(a) Forward pumping (b) Backward pumping

Fig. 4. Temperature increment as a function of z and r for (a) forward pumping and (b) backward pumping of Fiber A at 1 kW pump power and 1 W input signal power.

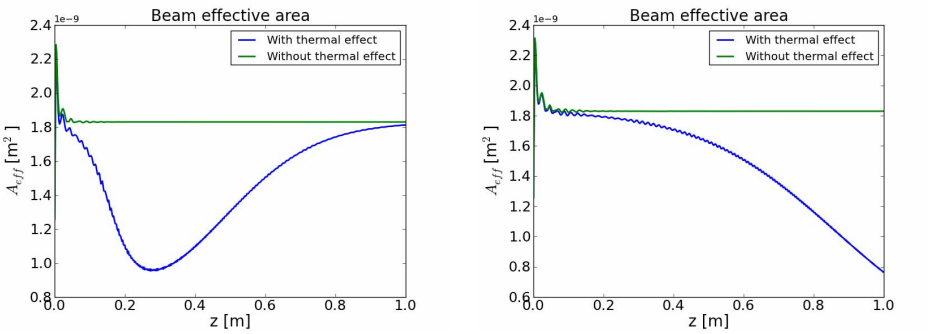

(a) Forward pumping (b) Backward pumping

Fig. 5. Beam effective area as a function of z for (a) forward pumping and (b) backward pumping of Fiber A at 1 kW pump power and 1 W input signal power.

Fiber A except that the core, inner cladding and outer diameters are 80 μm, 400 μm and 800 μm, respectively. It can be seen that as operating power on the order of 1 kW is reached, the thermal lensing effect starts to have a significant impact on the beam area and hence the severity of undesirable non-linear optical effects such as SPM, in particular for the backward pumped case, which is preferred over the forward pumped case due to the overall lower value of the B-integral and hence smaller impact of the aforementioned effects. Furthermore, the thermal

#152482 - $15.00 USD Received 5 Aug 2011; revised 19 Sep 2011; accepted 13 Oct 2011; published 10 Nov 2011

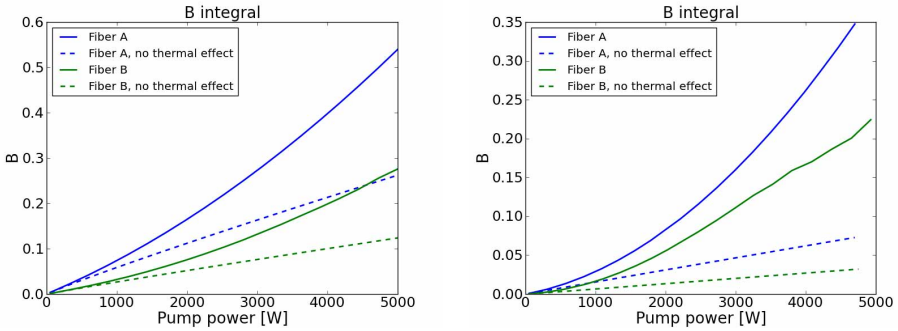

(a) Forward pumping (b) Backward pumping

Fig. 6. B integral as a function of pump power for (a) forward pumping and (b) backward pumping of Fiber A and B with 1 W input signal power. The dashed lines show the results with the thermal sensitivity η set to zero.

lensing effect changes the pump power dependence of the B integral from linear to super-linear. Comparing Fiber A to Fiber B, we see that the B integral for Fiber B, when the thermal lensing effect is taken into account, can exceed the expected B integral of Fiber A in the absence of thermal lensing, despite the fact that Fiber B has a core area 4 times larger than Fiber A. This occurs at a pump power of approximately 4.5 kW for forward pumping and 1 kW for backward pumping. However, it is also clear that even in the presence of a strong thermal lensing effect, increasing the core diameter still results in a significant reduction of the B integral and hence the severity of SPM.

3.2. Thermally induced multi-mode behavior

Another consequence of the thermally induced change in the refractive index of the fiber is that an otherwise single-mode fiber can be rendered effectively multi-mode. Such multi-mode behavior can have a negative impact on the output beam quality due to an uncontrollable drift of the relative phase between the excited modes [18]. It is also clear that the thermally induced multi-mode behavior will only occur beyond a certain power threshold, since the induced index change must be large enough to allow multiple guided modes to exist. Furthermore, once a higher order mode (HOM) is excited, the beating between the fundamental mode and HOM will create a thermally induced grating in the fiber. As discussed in [10], such a grating couples the two modes such that power may be transferred from the fundamental mode to the HOM.

Here we present the results of simulations that clearly show the above mentioned effects. We consider a 1 m long LMA SIF (Fiber C) with core, inner cladding and outer diameters of 80 μm, 400 μm and 800 μm, respectively. The index step between core and cladding is $\Delta n = 3 \times 10^{-5}$. While such a small index step is difficult to achieve in actual SIFs, it is obtainable using PCFs. The Yb concentration is 5×10^7 μm^{-3} and the pump and signal wavelength are 975 nm and 1030 nm. With these parameters, the V-parameter for the SIF is 2.28 and the fiber is thus single-mode by design. The pump power is 5 kW and the input signal power is 50 W. Figure 7 shows the signal and pump power as a function of z for both forward and backward pumping. The lower Yb concentration compared to the simulations of Fiber A and B in section 3.1 reduces the efficiency of the amplifier. We also note the presence of small oscillations of the signal power near the output, which are likely due to excitation of radiation modes.

Considering the effective area of the beam as a function of z shown in Fig. 8, we observe strong oscillations of the effective area, which would not occur if the signal was guided by a

#152482 - $15.00 USD Received 5 Aug 2011; revised 19 Sep 2011; accepted 13 Oct 2011; published 10 Nov 2011

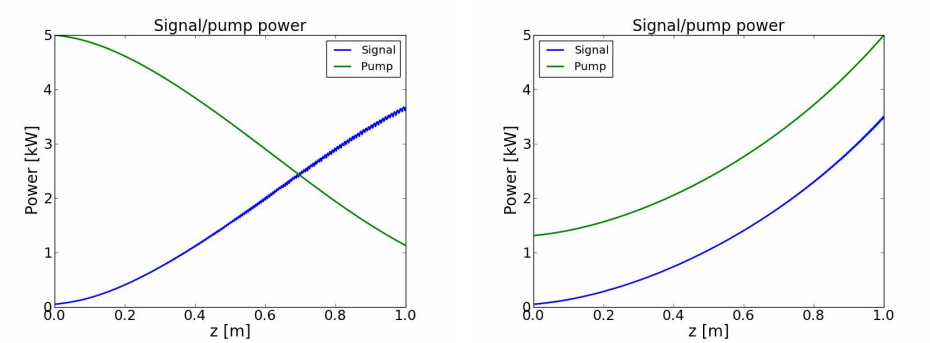

(a) Forward pumping (b) Backward pumping

Fig. 7. Signal and pump power as a function of z for (a) forward pumping and (b) backward pumping of Fiber C.

single mode and which therefore are a direct consequence of thermally induced multi-mode behavior. These oscillations are also seen in the temperature, shown in Fig. 9, and the excited state population, shown in Fig. 10.

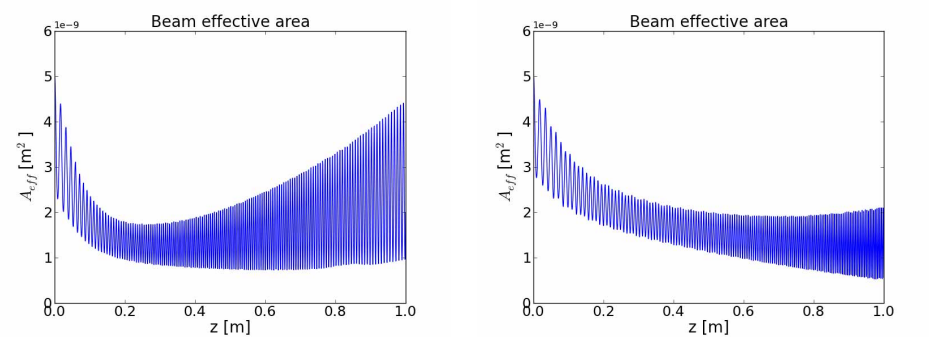

(a) Forward pumping (b) Backward pumping

Fig. 8. Beam effective area as a function of z for (a) forward pumping and (b) backward pumping of Fiber C at 5 kW pump power and 50 W input signal power.

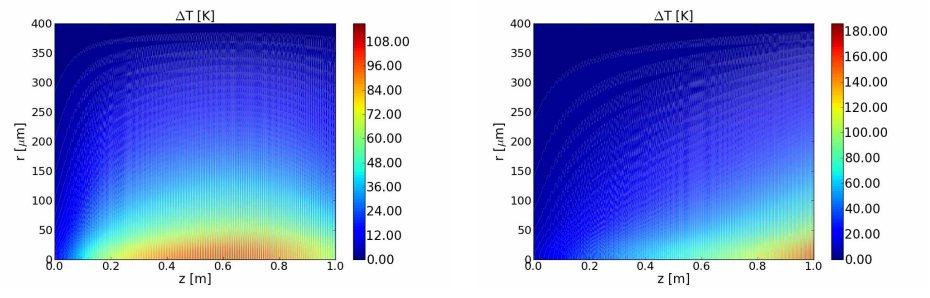

(a) Forward pumping (b) Backward pumping

Fig. 9. Temperature increment as a function of z and r for (a) forward pumping and (b) backward pumping of Fiber C at 5 kW pump power and 50 W input signal power.

#152482 - $15.00 USD Received 5 Aug 2011; revised 19 Sep 2011; accepted 13 Oct 2011; published 10 Nov 2011

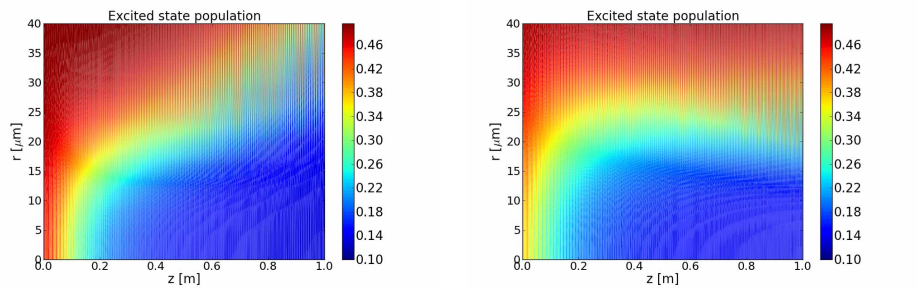

(a) Forward pumping (b) Backward pumping

Fig. 10. Excited state population as a function of z and r for (a) forward pumping and (b) backward pumping of Fiber C at 5 kW pump power and 50 W input signal power.

To provide additional insight into the nature of these oscillations, we decompose the signal field in local modes at each z position by solving the eigenvalue problem

$$\frac{\partial^2\Psi}{\partial r^2}+\frac{1}{r}\frac{\partial\Psi}{\partial r}+k_0^2\left[\varepsilon(r)+\Delta\varepsilon(r,z)\right]\Psi(r,z)=\beta^2(z)\Psi(r,z), \tag{23}$$

and computing the overlap between the normalized modes Ψ and the signal field. This overlap is given by

$$a_i(z)=\langle\Psi_i|E_s\rangle, \tag{24}$$

where the inner product is defined as

$$\langle\Psi|\Phi\rangle=\int_0^\infty\Psi^*(r)\Phi(r)r\mathrm{d}r. \tag{25}$$

The radial profiles of the fundamental and higher-order local modes at a given distance along Fiber C are calculated numerically from Eq. (23) using the thermally perturbed refractive index profiles, examples of which are shown in Fig. 11. The initial ($z=0$ m) mode profiles, plotted in Fig. 12, clearly show that several guided modes are present at the signal input. The launched signal can thus excite these higher-order local modes and the fiber is effectively multi-mode. The number of guided local modes may of course vary along the z axis as the temperature profile, and thus the refractive index perturbation, changes. Since our model is limited to cylindrically symmetric fields, we do not consider non-symmetric local modes, although such modes would certainly be expected to become guided under the present conditions. For comparison, we also plot the local mode profiles at the output end ($z=1$ m) of the fiber in Fig. 13. In the backward pumped case, the modes are more strongly confined due to the strong thermal lensing effect compared to the forward pumped case.

The local mode content $A_i(z)$ of the signal field is then defined to be

$$A_i(z)=\frac{|a_i(z)|^2}{\langle E_s|E_s\rangle} \tag{26}$$

and is plotted in Fig. 14. It is clear that in both the forward and backward pumped configurations, the input signal excites a small amount of the first higher-order local mode. The beating of these two modes creates the oscillations seen in the beam effective area shown in Fig. 8, and the associated intensity variation leads to the periodic variation of the population inversion seen in Fig. 10. Since the thermal load, given by Eq. (18), also depends on the signal intensity and population inversion, the temperature also exhibits a periodic variation as seen in Fig. 9. This

#152482 - $15.00 USD Received 5 Aug 2011; revised 19 Sep 2011; accepted 13 Oct 2011; published 10 Nov 2011

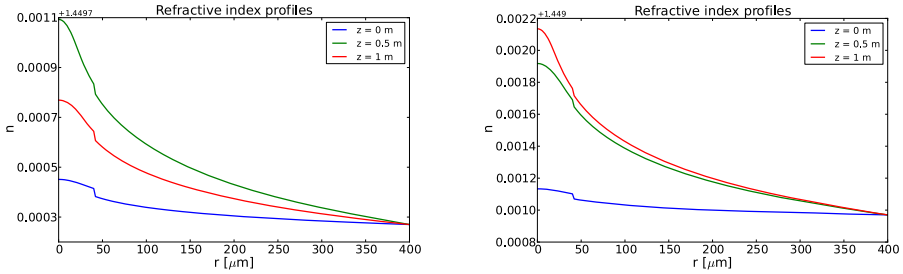

(a) Forward pumping (b) Backward pumping

Fig. 11. Thermally perturbed refractive index profiles at various z for (a) forward pumping and (b) backward pumping of Fiber C at 5 kW pump power and 50 W input signal power.

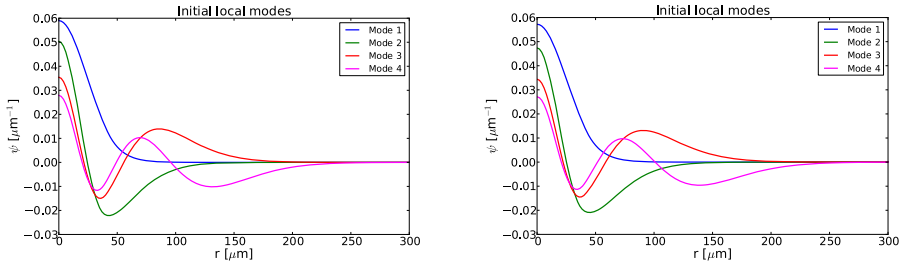

(a) Forward pumping (b) Backward pumping

Fig. 12. Initial $(z = 0)$ local modes for (a) forward pumping and (b) backward pumping of Fiber C at 5 kW pump power and 50 W input signal power.

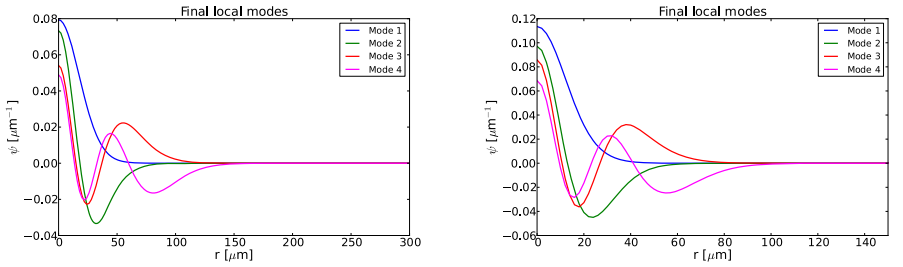

(a) Forward pumping (b) Backward pumping

Fig. 13. Final ($z = 1$ m) local modes for (a) forward pumping and (b) backward pumping of Fiber C at 5 kW pump power and 50 W input signal power.

temperature variation results in an index grating with a local period that matches the local beat length of the two local modes, and therefore provides coupling between the local modes. As is evident from Fig. 14, this leads to transfer of power from the fundamental to the higher-order local mode. We believe that this effective multi-mode behavior of the fiber amplifier under high-power operation can cause significant degradation of the output beam quality, since uncontrollable external perturbations such as temperature fluctuations and mechanical vibrations could conceivably change the relative phase of the local modes leading to significant changes in the output beam, as discussed in [18].

It is argued in [11] that the thermally induced refractive index grating, caused by mode-

#152482 - $15.00 USD Received 5 Aug 2011; revised 19 Sep 2011; accepted 13 Oct 2011; published 10 Nov 2011

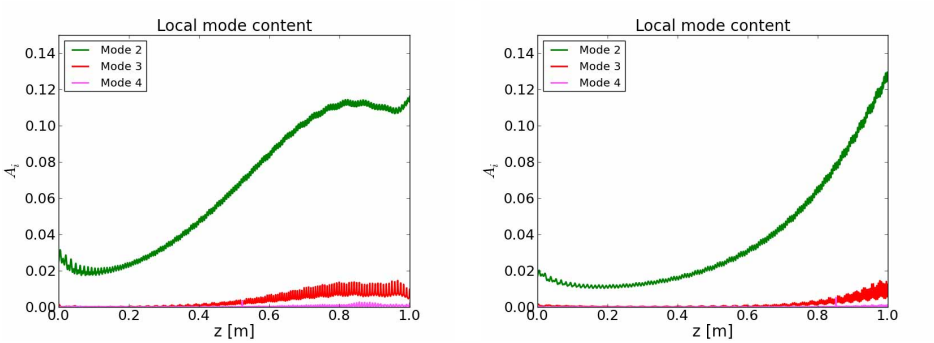

(a) Forward pumping (b) Backward pumping

Fig. 14. Local mode content as a function of z for (a) forward pumping and (b) backward pumping of Fiber C at 5 kW pump power and 50 W input signal power.

beating in a multi-mode fiber, cannot lead to coherent power transfer between two modes in a steady-state model of the thermal effect. The argument hinges on the left/right mirror symmetry of the mode interference pattern and the induced refractive index grating, and claims that a phase lag, which can be caused by the non-zero thermal diffusion time, is required to allow power transfer between the modes. Considering this argument, it is surprising that power transfer between the local modes in our model is observed, since our model is a steady-state model. While we do not disagree with the argument presented in [11], we note that it does not apply to the situations we are considering in this paper. This is because the temperature changes significantly over a short distance, as is evident from Fig. 9, and hence the local modes and their associated propagation constants change significantly over a short distance, as can be seen by comparing Fig. 12 and Fig. 13. This causes the periodicity of the induced refractive index grating to vary with z, and therefore breaks the left/right mirror symmetry which is the core of the argument in [11]. Power transfer between the local modes of the fiber thus cannot be ruled out at high operating power, even with a steady-state model, and indeed the results presented in Fig. 14 clearly show a significant power transfer from the fundamental to the first higher-order local mode.

To investigate the impact of gain saturation and pump depletion on the effective multi-mode behavior, we have simulated a fiber amplifier (Fiber D) with the same design as Fiber C, except that the Ytterbium concentration is increased to 10^8 μm^{-3} and the length of the fiber is increased to 1.5 m. The input pump and signal power is 2000 W and 50 W, respectively. As can be seen from the plots of the signal and pump power, shown in Fig. 15, the pump is completely depleted in both the forward and backward pumped cases. An interesting observation is that the signal power decreases significantly beyond 1 m in the forward pumped case. To understand the mechanism responsible for this decrease, we again consider the decomposition of the signal field into local modes, shown in Fig. 16, and the temperature distribution of the fiber, shown in Fig. 17. It is clear that the first higher-order local mode is strongly excited in the forward pumped case, but also that the signal gradually returns to the fundamental local mode beyond 1 m, which coincides with the decrease in signal power and temperature. Recalling that we have employed a transparent boundary condition in our algorithm and considering the definition of the local mode content given in Eq. (26), it is clear that the reason for the loss of signal power is due to the fact that the higher-order local mode evolves from a guided mode into a radiation mode as the radial temperature gradient decreases. The higher-order local mode content of the signal is thus lost beyond 1 m. Another source of the loss of signal power beyond 1 m is of

#152482 - $15.00 USD Received 5 Aug 2011; revised 19 Sep 2011; accepted 13 Oct 2011; published 10 Nov 2011

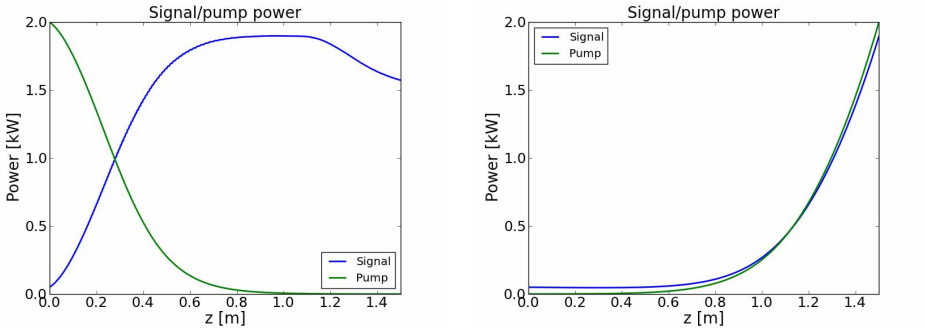

(a) Forward pumping (b) Backward pumping

Fig. 15. Signal and pump power as a function of z for (a) forward pumping and (b) backward pumping of Fiber D.

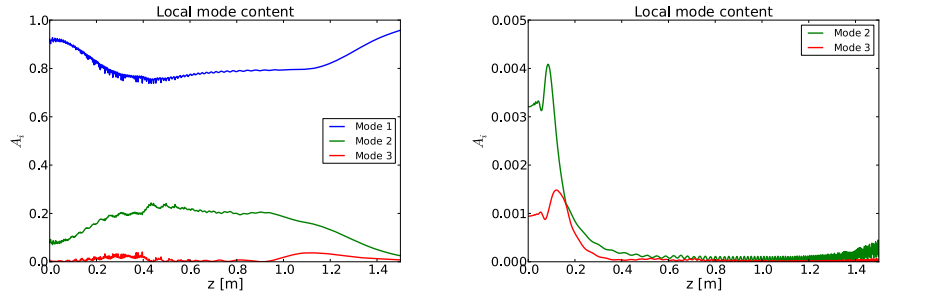

(a) Forward pumping (b) Backward pumping

Fig. 16. Local mode content as a function of z for (a) forward pumping and (b) backward pumping of Fiber D at 2 kW pump power and 50 W input signal power.

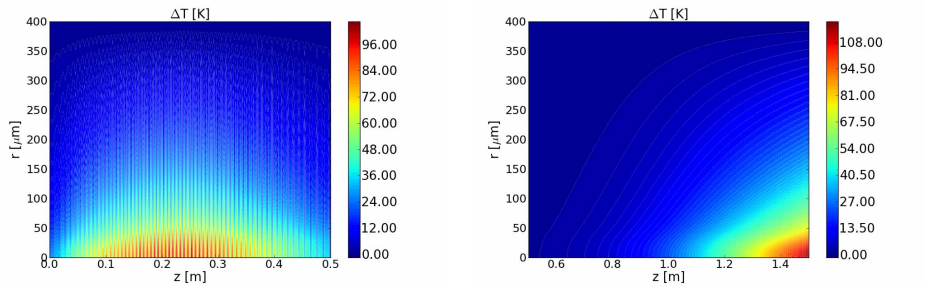

(a) Forward pumping (b) Backward pumping

Fig. 17. Temperature increment as a function of z and r for (a) forward pumping and (b) backward pumping of Fiber D at 2 kW pump power and 50 W input signal power.

course spontaneous emission from the excited state of the Ytterbium ions. However, this loss is quite small due to the relatively long lifetime of the excited state. We have verified that the signal power loss is dominated by the evolution of the higher-order local modes from guided to non-guided by simulating Fiber D without the thermal effect, which shows negligible signal power loss.

#152482 - $15.00 USD Received 5 Aug 2011; revised 19 Sep 2011; accepted 13 Oct 2011; published 10 Nov 2011

In the backward pumped configuration, there is practically no thermal gradient at the signal input, since the pump is depleted, and hence there is only one guided local mode, with HOMs being non-guided. The signal is thus coupled into this single guided mode, and consequently no beating pattern is created. As the temperature gradient increases along with the signal power, multiple guided local modes appear, but the signal is seen to adiabatically follow the fundamental local mode, with only negligible excitation of HOMs. Ideally, the output beam quality should thus be comparable to a true single-mode fiber in this case.

Finally, we have investigated the power dependence of the effective multi-mode behavior by calculating the local mode content at the output of Fiber C for varying input pump and signal power in a forward pumped configuration. The pump power is varied from 100 W to 5 kW, with an input signal power of 1% of the pump power. The results are shown in Fig. 18 which shows the higher-order local mode content at the output as a function of pump power. We find

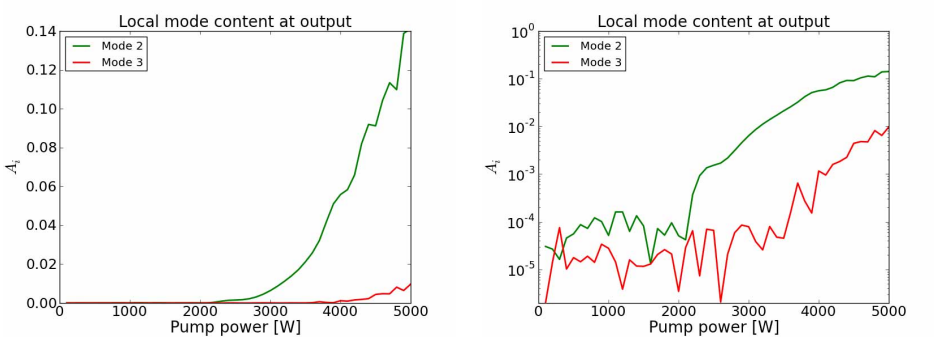

(a) Linear scale (b) Log scale

Fig. 18. Local mode content at the output as a function of pump power for Fiber C on (a) linear scale and (b) log scale.

that the first higher-order local mode content increases dramatically at pump powers greater than 2 kW, with a corresponding input signal power of 20 W. We note that beam instability issues in large core fiber amplifiers have been reported to occur at power levels from a few hundred W to around 1 kW average power [7, 9]. These fibers are, however, not strictly single-mode, which can lead to thermally induced coupling between the fundamental and higher-order modes, as discussed in [10, 11], without the need for a sufficiently strong thermal effect to create effective multi-mode behavior. Furthermore, our model can only describe symmetric local modes, and we expect that non-symmetric local modes become guided at much lower power. Our results thus show that even under the idealized conditions of true single-mode fiber design and a perfectly symmetric input signal beam profile, which prevents excitation of any asymmetric higher-order local modes, the output signal can be contaminated by higher-order modes at power levels which have been demonstrated.

4. Conclusion

We have developed a beam propagation model of high-power Yb-doped fiber amplifiers. The heating of the fiber due to the quantum defect associated with the gain medium, as well as transverse hole burning, is taken fully into account. The model is limited to cylindrically symmetric signal fields, leading to a very fast implementation that permits efficient simulation of backward pumped amplifiers. The model was used to study the thermo-optical effects in LMA single-mode amplifiers, and it was found that the large radial temperature gradient results in a thermal lensing effect, which significantly decreases the effective area of the beam, leading

#152482 - $15.00 USD Received 5 Aug 2011; revised 19 Sep 2011; accepted 13 Oct 2011; published 10 Nov 2011

to higher peak intensity. Furthermore, it was found that the thermal effect can become large enough to induce an effective multi-mode behavior, which can be quantified by decomposing the signal beam profile into local modes. If a higher-order local mode is excited at the signal input, the mode beating between the fundamental and higher-order local modes can set up a periodic longitudinal temperature variation, leading to a refractive index grating which can transfer power from the fundamental to the higher-order local mode. As discussed in [18], the excitation of higher-order modes may be detrimental to the output beam quality, and fiber amplifier designs should seek to avoid such behavior. Our results show that it is possible to reduce the thermally induced higher-order local mode content in nominally single-mode fibers if the thermal load is weak enough at the signal input. This may be possible to achieve in backward pumped fiber amplifiers with sufficient length and Yb-doping to effectively absorb the pump. Our results also indicate that as the thermal effect diminishes due to gain saturation in a forward pumped amplifier, any signal power contained in a higher-order local mode will remain in that mode as it turns into a non-guided mode. Finally, we investigated the power-dependence of the thermally-induced multi-mode behavior and found that the higher-order local mode content increases dramatically with operating power beyond a certain threshold power. Since our model is limited to cylindrically symmetric fields, we cannot investigate a situation in which the input beam profile is shifted or tilted relative to the symmetry axis of the fiber, which could lead to excitation of asymmetric higher-order local modes. We therefore expect the threshold power obtained by our model to be an upper-threshold, applicable under idealized conditions in which no excitation of asymmetric higher-order local modes occurs.

Acknowledgments

This work was supported by the Danish Research Council for Technology and Production.

#152482 - $15.00 USD Received 5 Aug 2011; revised 19 Sep 2011; accepted 13 Oct 2011; published 10 Nov 2011